Mon. Not. R. Astron. Soc. **307**, 984–992 (1999)

Coulomb corrections to the equation of state of nuclear statistical equilibrium matter: implications for SNIa nucleosynthesis and the accretion-induced collapse of white dwarfs

E. Bravo[1,2★] and D. García-Senz[1,2]

[1]*Departament de Física i Enginyeria Nuclear, Universitat Politècnica de Catalunya, Av Diagonal 647, 08028 Barcelona, Spain*[†]
[2]*Institut d'Estudis Espacials de Catalunya, Ed. Nexus 104, Gran Capità 2–4, 08034 Barcelona, Spain*[‡]

Accepted 1999 March 25. Received 1999 March 15; in original form 1998 August 4

ABSTRACT

Coulomb corrections to the equation of state of degenerate matter are usually neglected in high-temperature regimes, owing to the inverse dependence of the plasma coupling constant, Γ, on temperature. However, nuclear statistical equilibrium matter is characterized by a large abundance by mass of large-Z (iron group) nuclei. It is found that Coulomb corrections to the ion ideal gas equation of state of matter in nuclear statistical equilibrium are important at temperatures $T \lesssim 5\text{–}10 \times 10^9$ K and densities $\rho \gtrsim 10^8\,\mathrm{g\,cm^{-3}}$. At a temperature $T = 8.5 \times 10^9$ K and a density $\rho = 8 \times 10^9\,\mathrm{g\,cm^{-3}}$, the neutronization rate is larger by $\gtrsim$28 per cent when Coulomb corrections are included. However, the conductive velocity of a thermonuclear deflagration wave in C–O drops by $\sim$16 per cent when Coulomb corrections to the heat capacity are taken into account. The implications for SNIa models and nucleosynthesis, and also for the accretion-induced collapse of white dwarfs, are discussed. Particularly relevant is the result that the minimum density for collapse of a white dwarf to a neutron star is shifted down to $5.5\text{–}6 \times 10^9\,\mathrm{g\,cm^{-3}}$, a value substantially lower than previously thought.

Key words: equation of state – nuclear reactions, nucleosynthesis, abundances – stars: neutron – supernovae: general – white dwarfs.

1 INTRODUCTION

Since the pioneering work of Salpeter (1961) dealing with the corrections to an ideal plasma at zero temperature, non-ideal effects and, especially, Coulomb corrections have been incorporated into the equation of state (EOS) of stellar evolutionary codes. As they constitute a first-order correction to the ideal gas EOS, Coulomb corrections significantly influence the evolution and structure of bodies near hydrostatic equilibrium, where a small but non-negligible variation in the pressure–density relationship can lead to a substantial change in the structure. Good examples are red giants and white dwarfs. In massive stars near the end of their life, iron core masses lower by $\sim$5–10 per cent are obtained when Coulomb corrections are included in the EOS, compared with calculations without corrections (Woosley & Weaver 1988). The effects of Coulomb corrections on heat capacity and pressure, in conditions appropriate to follow the evolution of presupernova and supernova explosions of massive stars, have been studied by several authors (Hillebrandt, Nomoto & Wolff 1984; Nomoto & Hashimoto 1988; Nomoto, Thielemann & Yokoi 1984). The cooling time and the Chandrasekhar mass of white dwarfs are also sensitive to the inclusion of the electrostatic corrections to the EOS.

The importance of Coulomb corrections in a finite temperature plasma is measured by the plasma coupling constant, $\Gamma_\mathrm{i} = (Ze)^2/r_\mathrm{i}kT$, where r_i is the mean interionic distance. Because of the inverse dependence of Γ_i on temperature, these corrections have been applied preferably to moderately cold material at high density, such as that found in white dwarf interiors or in the cores of giant stars. In situations that involve high-temperature matter (greater than a few times 10^9 K), the corrections have usually been neglected (Epstein & Arnett 1975; Bruenn 1972) or only partially included (Timmes & Woosley 1992).

Matter in nuclear statistical equilibrium (NSE) is characterized by a large abundance of iron peak nuclei. In spite of the high temperature needed to reach NSE, the large value of the atomic number, Z, of these nuclei makes Coulomb corrections relevant in this regime. Mochkovitch & Nomoto (1986) pointed out the importance of including the Coulomb correction to the chemical potential of nuclei in NSE in order to obtain their relative abundances accurately. Later, Hix & Thielemann (1996) did include Coulomb corrections in their network calculations of Si-

★ E-mail: bravo@fen.upc.es
† World Wide Web address: http://www-fen.upc.es
‡ World Wide Web address: http://www.ieec.fcr.es

burning. However, thorough research into the consequences of including Coulomb corrections in the EOS of matter in NSE has not been undertaken until now.

The purpose of the present paper is to determine the actual relevancy of Coulomb corrections for the distribution of nuclei in NSE, and to calibrate the consequences for white dwarf evolution. The next section is devoted to the introduction of the terms in which Coulomb corrections are computed, and how they are taken into account for the calculation of NSE abundances. In Section 3 we discuss the consequences of Coulomb corrections in NSE matter at high temperature, paying special attention to the velocity of propagation of thermonuclear conductive laminar flames and to the rate of change of the electron mole number in NSE. Sections 4 and 5 are dedicated to evaluating the impact of Coulomb corrections on the evolution and nucleosynthesis of type Ia supernova (SNIa) explosions, and on the critical density for collapse of a white dwarf to a neutron star, respectively. Finally, our conclusions are outlined in Section 6.

2 COULOMB CORRECTIONS AND NUCLEAR STATISTICAL EQUILIBRIUM

For a one-component plasma (OCP), the corrections to the ideal EOS resulting from the interaction of ions within a uniform electron background are a function of the ion coupling parameter, $\Gamma_{\rm i}$. We adopted the expression obtained by Ogata & Ichimaru (1987) for the Helmholtz free energy per ion in the regime $\Gamma_{\rm i} > 1$:

$$\frac{f_{\rm C}}{kT} = a\Gamma_{\rm i} + 4\left(b\Gamma_{\rm i}^{1/4} - c\Gamma_{\rm i}^{-1/4}\right) + d\ln\Gamma_{\rm i} - o, \tag{1}$$

where the values of the parameters a, b, c, d and o are given by Ogata & Ichimaru (1987). Note that the leading term for $f_{\rm C}$ in the above expression is independent of temperature. For $\Gamma_{\rm i} < 1$, the dependence proposed by Yakoblev & Shalybkov (1989) was adopted:

$$\frac{f_{\rm C}}{kT} = -\frac{1}{\sqrt{3}}\Gamma_{\rm i}^{3/2} + \frac{\beta}{\gamma}\Gamma_{\rm i}^{\gamma}. \tag{2}$$

The parameters β and γ were in order to enable a smooth transition from $\Gamma_{\rm i} > 1$ to $\Gamma_{\rm i} < 1$, while preserving the Debye–Huckel limit for $\Gamma_{\rm i} \ll 1$ (Yakovlev & Shalybkov 1989). The respective expressions for the corrections to the chemical potential of the ions, $\mu_{\rm C}$, in both regimes can be easily calculated from the above equations.

The abundances of nuclei in NSE were computed as a function of temperature, density and electron mole number, $Y_{\rm e}$, following the method of Clifford & Tayler (1965). From the condition of equilibrium between each nucleus i (with atomic number Z_i and baryonic number A_i) and free particles

$$\mu_i = Z_i\mu_{\rm p} + (A_i - Z_i)\mu_{\rm n}, \tag{3}$$

and the expressions for the chemical potentials (rest mass included), the number density of nucleus i, n_i, can be written as

$$n_i = \frac{g_i A_i^{3/2}}{2^{A_i}\theta^{A_i-1}} n_{\rm p}^{Z_i} n_{\rm n}^{A_i-Z_i} \exp\left(-\frac{Q_i}{kT}\right), \tag{4}$$

$$\theta = \left(\frac{2\pi m_{\rm H} kT}{h^2}\right)^{3/2}, \tag{5}$$

where $n_{\rm p}$ and $n_{\rm n}$ stand for the number density of free protons and neutrons. The values of $n_{\rm p}$ and $n_{\rm n}$ can be found by imposing the conservation of charge and baryon number. In the above expression, Q_i is the difference between the chemical potential of nucleus i and that of its nucleons, excluding the ideal gas contribution. Neglecting the Coulomb correction to the chemical potential leads to $Q_{i0} = [m_i - Z_i m_{\rm p} - (A_i - Z_i)m_{\rm n}]c^2$. This is the approximation usually adopted to compute NSE abundance distributions. When Coulomb corrections are taken into account, the expression for Q_i changes to

$$Q_i = [m_i - Z_i m_{\rm p} - (A_i - Z_i)m_{\rm n}]c^2 + \mu_{i,{\rm C}} - Z_i\mu_{\rm p,C}. \tag{6}$$

As the Coulomb correction to the chemical potential is negative, and Γ depends on $Z_i^{5/3}$, its inclusion shifts the abundance distribution to favour heavier nuclei (Mochkovitch & Nomoto 1986). Generally speaking, nuclear statistical equilibrium matter is richer in nuclei with greater nuclear binding energy per baryon, because of the contribution of the nuclear mass excess in the expression for Q_i. However, the Coulomb correction is insensitive to nuclear structure details. Thus, inclusion of the Coulomb chemical potential slightly equalizes the abundance distribution in NSE. For illustration purposes, in Table 1 the quantity $100 \times [\Delta b_i - \Delta b(^{56}{\rm Fe})]/[b_{i0} - b_0(^{56}{\rm Fe})]$ is given for some isotopes of Co and Fe, at a density of $8 \times 10^9\,{\rm g\,cm^{-3}}$ and a temperature of $10^{10}\,{\rm K}$. In the previous expression, $b_{i0} \equiv Q_{i0}/A_i$ is the nuclear binding energy per baryon, while $b_i \equiv Q_i/A_i$ is the Coulomb-corrected binding energy per baryon. It can be seen that, in general, inclusion of the Coulomb correction decreases the difference in binding energy with respect to ^{56}Fe, although there are exceptions, as is the case for ^{57}Fe.

Table 1. Per cent variation of binding energy per baryon relative to ^{56}Fe.

^{55}Co	^{56}Co	^{57}Co	^{58}Co	^{54}Fe	^{55}Fe	^{57}Fe
−7	−7	−10	−7	−6	−4	+8

For a multicomponent plasma (MCP), such as that resulting from NSE, Coulomb corrections to the EOS are usually calculated following the additive approximation. In this approximation, the free energy is computed as the sum of the individual free energy of each species computed as if it were an OCP. In the sum, the free energy of each species is weighted by its molar fraction in the mixture. In NSE the number of nuclei with abundances significantly greater than zero can be very large (tens or even hundreds, depending on the density, temperature and electron mole number), which makes the computation of individual OCP Coulomb corrections for each nucleus very inefficient for any stellar evolutionary code. In the hydrodynamical calculations presented in this paper we chose instead to compute Coulomb corrections in NSE through a table, which has the values of the appropriate means of functions of Z, as follows. From the additive approximation, and the expression for the Coulomb correction to the free energy for $\Gamma_{\rm i} > 1$,

$$\frac{f_{\rm C}}{kT} = a\Gamma_{\rm e}\langle Z^{5/3}\rangle + 4\left(b\Gamma_{\rm e}^{1/4}\langle Z^{5/12}\rangle - c\Gamma_{\rm e}^{-1/4}\langle Z^{-5/12}\rangle\right) + d\ln\Gamma_{\rm e} + \frac{5}{3}d\langle\ln Z\rangle - o, \tag{7}$$

$$\Gamma_{\rm e} = \frac{e^2}{a_{\rm e}kT}, \tag{8}$$

$$a_{\rm e} = \left(\frac{3}{4\pi n_{\rm e}}\right)^{1/3}. \tag{9}$$

The means over NSE composition ($\langle Z^{5/3}\rangle$, $\langle Z^{5/12}\rangle$, $\langle Z^{-5/12}\rangle$ and $\langle\ln Z\rangle$) were computed for a grid of temperatures, densities and electron mole numbers ($2 \times 10^9 \leqslant T \leqslant 4 \times 10^{10}\,{\rm K}$, $10^8 \leqslant \rho \leqslant$

$10^{12}\,\mathrm{g\,cm^{-3}}$, $0.40 \leqslant Y_e \leqslant 0.50$), and stored in a table. The table is dense enough for a linear interpolation in T, ρ and Y_e to provide the MCP Coulomb corrections in NSE with high accuracy and low computational cost (nearly equal to the OCP correction). The table is available to interested readers upon request to the authors. The table is also useful for the calculation of the MCP Coulomb corrections if the prescription by Hansen, Torrie & Vieillefosse (1977) is preferred. Hansen et al. calculate the MCP corrections with the OCP formulae, and an 'effective' charge,

$$Z_{\mathrm{eff}} = \langle Z\rangle^{1/6}\langle Z^{5/3}\rangle^{1/2}. \tag{10}$$

For completeness, the value of $\langle Z\rangle$ was also included in our table.

3 EFFECTS OF COULOMB CORRECTIONS AT HIGH TEMPERATURE

3.1 Conductive thermonuclear flames

The physics of laminar (conductive) flames is a crucial ingredient in thermonuclear supernova (SNIa) theory, and also in the scenario of the accretion-induced collapse of white dwarfs. The velocity of conductive deflagration fronts determines the evolution of the white dwarf immediately following central ignition and the time available for electron captures behind the front. The conductive velocity is determined by nuclear reaction kinetics, but also by the EOS of matter. The pressure exerted by nuclear ashes is responsible for pushing and accelerating the fuel through the front, while the heat capacity determines the evolution of temperature following heat conduction and nuclear energy release. Coulomb corrections to both pressure and heat capacity should be included in any modelling of the flame with a view to the calculation of the conductive velocity.

The conductive velocity of a C–O flame was determined by Timmes & Woosley (1992, hereafter TW), for temperature and density conditions appropriate to white dwarfs. In their paper, TW included electrostatic Coulomb corrections to the chemical potential, pressure and internal energy in the low-temperature, high-density regime, following Salpeter (1957). These are *zero-temperature corrections*, which do not include a Coulomb contribution to the heat capacity.

We carried out a numerical study aimed at obtaining a suitable correction factor for the conductive velocity values given by TW at several densities. In their paper, TW computed the conductive velocity using several different approximations to the deflagration front physics. Two formulations were regarded as 'fundamental', one being the integration of the equations of motion, energy and nuclear kinetics, and the other the integration of an energy diffusion equation together with the nuclear kinetics equations. In the latter method, the conductive deflagration front was assumed to be isobaric, which is justified in view of the very subsonic nature of the flame. What is relevant for our discussion is that both methods gave coherent results, thus enabling the recomputation of the conductive velocity by means of either of them. For simplicity, we chose to recompute the conductive velocity of a C–O flame using the energy diffusion method.

We have integrated the equation of energy together with a small nuclear network. As previously stated, the isobaric condition was imposed through the flame. The flame was initially represented by a step-like function. Afterwards, the integration of the equations was performed numerically, allowing the flame structure to relax to a steady state. At this point, the steady conductive velocity was determined. We included all Coulomb corrections for the EOS, but then repeated the calculations with only Salpeter's (1957) corrections, in order to compare the results. Our complete EOS includes partially degenerate electrons with pair corrections, ideal ion gas plus Coulomb corrections, and radiation. For the opacity, which is largely dominated by electrons, we followed Nandkumar & Pethick (1984), whose prescription compares well with that used by TW. The nuclear network we used was a simple α network from C to Si, plus protons, neutrons, α and Ni. The link between Si and Ni was established through relationships between quasi-statistical equilibrium groups. This is the same nine-nucleus network as was used by TW in some of their calculations. This nuclear network is the minimum needed to follow approximately the energetics of explosive carbon ignition, giving a front velocity that is a factor of 2 below that obtained with a larger network (TW). However, it is sufficient for the comparative task in hand, as we are not concerned with recomputing *absolute* conductive velocities, but rather *relative* corrections to the velocities given in TW. Furthermore, we can compare our results with those obtained by TW using the same simplified network. In their paper, TW reported a flame velocity of $113\,\mathrm{km\,s^{-1}}$ in C–O at $\rho = 6\times 10^9\,\mathrm{g\,cm^{-3}}$ using the nine-isotope network (see their table 5), while our value (with Salpeter-like Coulomb corrections) is $98\,\mathrm{km\,s^{-1}}$. Thus the comparison is satisfactory.

Our results for a density $\rho = 9\times 10^9\,\mathrm{g\,cm^{-3}}$ are summarized in Figs 1 and 2. Fig. 1 shows the evolution of the velocity of the conductive flame from the beginning of the calculation, through the relaxation of the flame structure, and up to its stabilization at a steady conductive velocity. The curves correspond to the velocities determined without Coulomb corrections (long-dashed line), including zero-temperature Coulomb corrections, as in TW (short-dashed line), and including complete Coulomb corrections in the linear mixing approximation, as explained in the previous

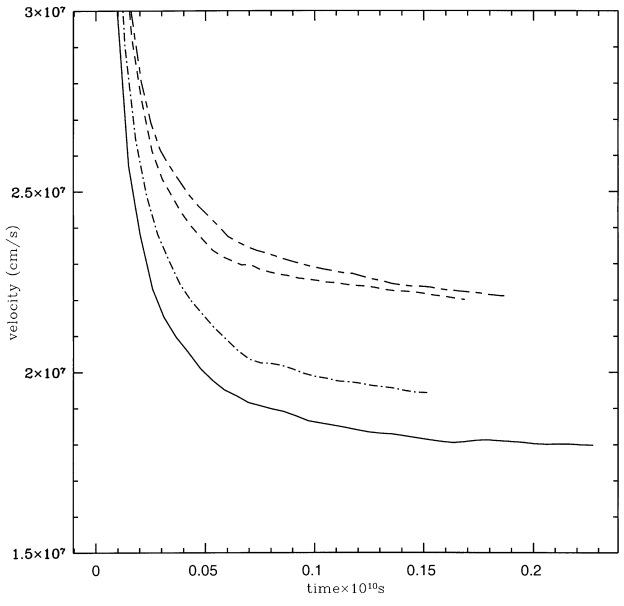

Figure 1. Conductive velocity as a function of time elapsed from the beginning of the numerical computation. Four lines are shown, corresponding to different levels of Coulomb corrections to the EOS (see text for explanation). The velocity is computed as the distance covered by the flame divided by the total elapsed time. The flame position was advanced a meshpoint when its temperature exceeded an arbitrarily chosen value (here 2×10^9 K), thus the speed was high at the beginning, but asymptotically reached a steady value after the flame moved a distance of several times its own width.

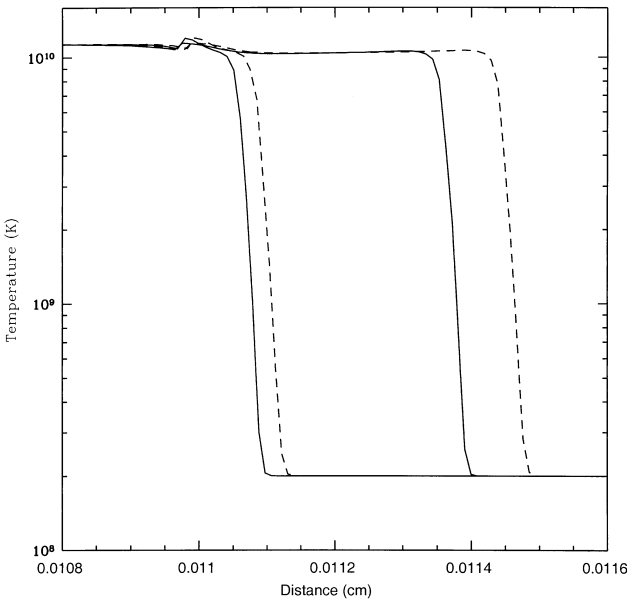

Figure 2. Thermal structure of the conductive flame front with (solid line) and without (dashed line) Coulomb corrections to the heat capacity. The leftmost profiles correspond to a time shortly after the beginning of the calculation, while the rightmost profiles correspond to 1.6×10^{-11} s later.

section (dot–dashed line) and in Hansen's approximation (solid line). It can be seen that there is little difference between applying Coulomb corrections only to the ion pressure (as in TW) and not applying them at all. However, when the Coulomb contribution to the specific heat was also taken into account the flame velocity dropped (at its final steady-state value) by about 12 per cent. If Hansen's prescription is used, the effect is even more pronounced, giving rise to a correction to the TW conductive velocity of about 16 per cent. Fig. 2 shows the conductive front structure for both calculations: with Coulomb corrections as in TW (dashed line), and with full Coulomb corrections in the linear approximation (solid line), for a time shortly after the beginning of the calculation (left) and 1.6×10^{-11} s later (right). It can clearly be appreciated that the velocity is greater in the calculation without Coulomb corrections to the heat capacity. The small bump just behind the front in the left-hand curves is caused by incompleteness of the relaxation process of the front structure. It disappears completely in the later (steady-state) curves.

The effect of the Coulomb correction on the heat capacity decreases with decreasing density. The corresponding corrected conductive velocity can be fitted in the range $5 \times 10^7 \leqslant \rho \leqslant 10^{10}$ g cm^{-3} by the following function of density (for a 50–50 per cent C–O composition):

$$\frac{v_{\rm cond}}{v_{\rm TW}} = 0.894 - 0.0316 \ln \rho_9, \qquad (11)$$

where ρ_9 is the density in units of 10^9 g cm^{-3}, and $v_{\rm TW}$ is the value of the conductive velocity given in TW. For $\rho_9 > 10$, the correction can be taken as fixed at -14 per cent, while for $\rho < 5 \times 10^7$ g cm^{-3} the correction can be considered negligible. The dependence of the correction factor on initial chemical composition is less clear. A high initial carbon abundance leads to a sharper rise in temperature, thus building elements with higher Z, while the opposite is true for a fuel composed mainly of oxygen. As $\Gamma_{\rm i} \propto Z^{5/3}/T$, the two effects partially compensate each other and the resulting Coulomb corrections are not significantly different from the case with $X_{\rm C} = X_{\rm O} = 0.5$. We computed the conductive velocities again for various initial carbon abundances. At a density of $\rho_9 = 9$, the reduction of the conductive velocity was as follows: 16 per cent for $X_{\rm C} = 0.5$, 12 per cent for $X_{\rm C} = 1$ and 10 per cent for $X_{\rm C} = 0.2$.

3.2 Neutronization rate of matter in NSE

During the dynamical phases of evolution of supernovae and neutron star formation, matter neutronization is provided mainly by electron captures on NSE nuclei. Neutronization rates are an essential ingredient to follow the aforementioned processes. They not only determine the composition, but their effects include depressurization resulting from electron removal, decrease of the effective length scale of Rayleigh–Taylor instability (Timmes & Woosley 1992), and others. Bulk neutronization rates in NSE matter were calculated by Epstein & Arnett (1975), who provided simple and useful analytic expressions for $\dot{Y}_{\rm e}$, although they did not include electrostatic corrections to the chemical potentials of nuclei. Neutronization rates in NSE are affected in two different ways by Coulomb corrections: the abundance distribution of nuclei is changed, and the specific electron capture rate for each nucleus at a given density is also modified.

The change in the electron capture rate for a given nucleus is caused by the shift in the threshold density for capture, as the chemical potentials of nuclei are modified by Coulomb interactions. The methodology for the inclusion of this shift in the calculation of electron capture rates has been given by Couch & Loumos (1974). Basically, Coulomb effects can be taken into account by working with an effective Q value of the transition, increased by the difference between the chemical potentials of the nuclei involved. Their relevance for the issue of explosion/collapse of massive O–Ne–Mg cores, where the precise threshold density at which electron captures begin is a crucial parameter, was recognized by Gutierrez et al. (1996). However, in the conditions relevant for SNIa explosions and the accretion-induced collapse (AIC) of C–O white dwarfs, the bulk of electron captures have large positive nuclear Q values, while electron Fermi energies are of order ~5–8 MeV. As the shift of the Q value is of order ~300–500 keV (Couch & Loumos 1974), it is not expected to have a large impact on the overall rate of neutronization of NSE matter. For instance, for a nucleus such as ^{55}Co, at 2×10^9 g cm^{-3} the electron capture rate is reduced by ~9 per cent owing to the Coulomb shift of the Q value, while at 8×10^9 g cm^{-3} the reduction is only ~10 percent. For other nuclei that contribute considerably to the bulk NSE neutronization rate the figures are similar.

The nuclei that are dominant in the bulk rate of neutronization of matter in NSE are not, generally speaking, the most abundant ones. The reason for this is that the most abundant nuclei are usually also the most tightly bound among those with Z/A close to $Y_{\rm e}$, and they are consequently not very prone to making a weak transition. At the conditions at which the bulk of neutronization occurs in SNIa and the AIC of a white dwarf (that is, densities well above 10^9 g cm^{-3}) the nuclei that contribute the most to the neutronization in NSE are p, Co isotopes, and some isotopes of Fe and Mn. As was shown in Section 2 (Table 1), Co isotopes are generally favoured by the inclusion of Coulomb corrections to the EOS. One can then expect that inclusion of those corrections will lead to an increase in the bulk neutronization rate of matter in NSE. Fig. 3 shows the abundances in NSE of the main e-capture

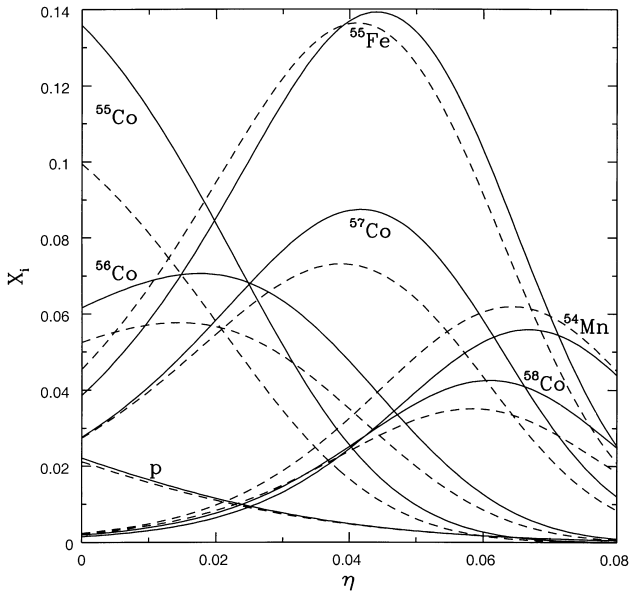

Figure 3. NSE abundances of the main e-capture nuclei as a function of the neutron excess, with (solid lines) and without (dashed lines) Coulomb corrections to the chemical potentials. The density is 2×10^9 g cm^{-3}.

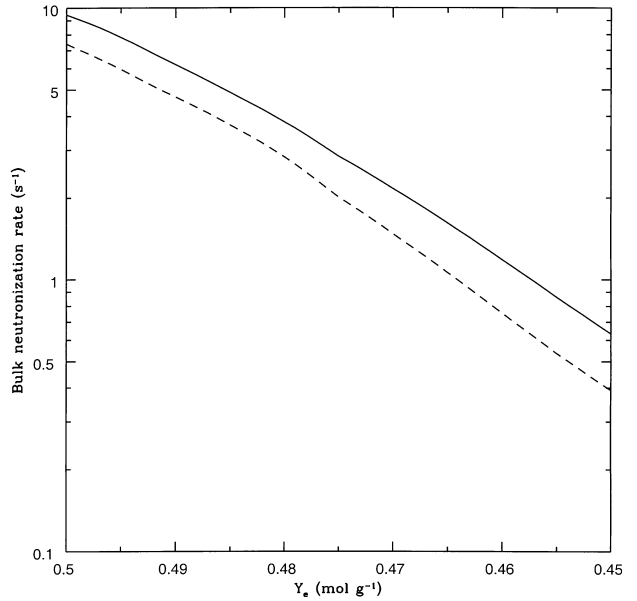

Figure 4. Bulk neutronization rate in NSE as a function of the electron mole number Y_e, with (solid line) and without (dashed lines) Coulomb corrections to the chemical potentials. The density is 8×10^9 g cm^{-3}.

nuclei, as a function of the neutron excess: $\eta = 1 - 2Y_e$, at $\rho = 2 \times 10^9$ g cm^{-3} and $T = 8 \times 10^9$ K. Solid lines are for Coulomb corrections included, while dashed lines are for NSE abundances calculated without Coulomb corrections to the chemical potentials. It can be seen how the abundances of Co isotopes are increased in the whole range covered by the figure, with increments up to ~35 per cent (^{55}Co at $\eta = 0$). The abundances of other nuclei, such as ^{55}Fe, are enhanced at large η, but depleted at low η, while proton abundance is rather insensitive to Coulomb corrections. From these figures, one can expect major increases in the bulk neutronization rate in NSE. While free protons are the main species responsible for matter neutronization in NSE from $\eta = 0$ to $\eta = 0.04$ when no Coulomb corrections are included, this role is assumed by ^{55}Co when the corrections are taken into account.

We computed the neutronization rate in NSE with and without Coulomb corrections. Individual weak interaction rates for each nucleus were calculated from Fuller, Fowler & Newman (1985). The results for a density $\rho = 8 \times 10^9$ g cm^{-3} are shown in Fig. 4. With Coulomb corrections the neutronization rate is faster, while its decrease with Y_e is less steep than without the corrections. At the aforementioned density, Coulomb corrections raise the bulk NSE neutronization rate by 28 per cent at $Y_e = 0.5$ mol g^{-1}, and by 72 per cent at $Y_e = 0.45$ mol g^{-1}.

From the above discussion, it is clear that Coulomb corrections in NSE matter should be taken into account whenever neutronization is a relevant physical process. Bulk neutronization rates are given by $\dot{Y}_e = \Sigma_i \lambda_i Z_i Y_i$, where λ_i is the weak interaction rate of nucleus i (negative for electron captures and β^+ decays) and Y_i is the usual molar fraction of nucleus i ($Y_i = n_i / \Sigma_j n_j A_j$). Individual electron capture rates for each nucleus, λ_i, at a given temperature and density can be calculated accurately enough from Fuller et al. (1985), as it has been shown that the shift in the threshold density for electron capture caused by Coulomb interactions introduces only a second-order correction in the neutronization rate for typical conditions in NSE matter. However, the abundance distribution of nuclei in NSE must be computed with the Coulomb corrections to the chemical potentials, i.e. with Q_i given by equation (6), and n_i by equations (4) and (5) and by $\Sigma_i n_i A_i = \rho_b$ and $(\Sigma_i n_i Z_i)/(\Sigma_i n_i A_i) = Y_e$. In the previous expressions ρ_b stands for the baryonic density, which is a conserved quantity in a closed system evolving at constant volume. The Coulomb part of the chemical potential of each nucleus, i, is given by

$$\mu_{i,C} = kT\left[a\Gamma_e Z_i^{5/3} + 4\left(b\Gamma_e^{1/4} Z_i^{5/12} - c\Gamma_e^{-1/4} Z_i^{-5/12}\right) + d \ln\left(\Gamma_e Z_i^{5/3}\right) - o\right], \quad (12)$$

for $\Gamma_i > 1$, with Γ_e given by equations (8) and (9).

As expected, both the bulk neutronization rate in NSE and the amount of correction resulting from electrostatic interactions are strongly dependent on density and electron mole number. The neutron excess achieved by a given mass results from its density history, basically from the competition between its hydrodynamic time and the characteristic time of neutronization. To analyse further the effect of Coulomb corrections on the final Y_e attained by a mass, we now make some assumptions to simplify the problem. Let us first assume that the bulk neutronization rate in NSE can be calculated with sufficient precision by a law of the form $\dot{Y}_e = -CY_e^a \rho^b$, with C, a and b constants. Let us also assume that, after incineration, the mass density decreases following an exponential law: $\rho = \rho_0 \exp(-t/\tau) \Rightarrow \dot{\rho} = -\rho/\tau$, where τ is its hydrodynamical time. Then, the following equation can be derived:

$$\frac{dY_e}{d\rho} = C\tau Y_e^a \rho^{b-1}, \quad (13)$$

which can be integrated to obtain

$$Y_e = \left[Y_0^{1-a} + \frac{C}{b}(1-a)\tau\left(\rho^b - \rho_0^b\right)\right]^{1/(1-a)}, \quad (14)$$

where Y_0 is the initial electron mole number, usually $Y_0 = 0.5$ mol g^{-1}. We obtained the following fits to the neutronization rate with, $\dot{Y}_{e,C}$, and without, $\dot{Y}_{e,noC}$, Coulomb corrections, in the

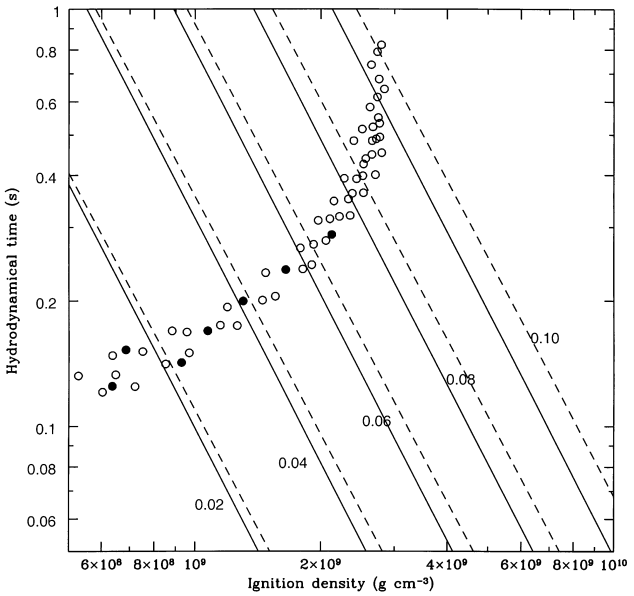

Figure 5. The final value of the neutron excess is shown as a function of the ignition density and the hydrodynamical time for the case with (solid lines) and without (dashed lines) Coulomb corrections. An initial value of $\eta_0 = 0$ has been assumed. Lines are labelled with the value of the neutron excess. Circles show the ignition density and expansion time for different mass shells of a particular SNIa deflagration model (see Section 4 for details). Filled circles mark the mass shells at 0.05, 0.10, 0.15, 0.20, 0.25, 0.30 and 0.35 $M_\odot$. Distance from the centre increases to the bottom and to the left.

range $0.45 \leqslant Y_e \leqslant 0.50\,\mathrm{mol\,g^{-1}}$, and around $\rho = 10^9\,\mathrm{g\,cm^{-3}}$:

$$\dot{Y}_{e,C} = -0.29\rho_9^{1.95}\left(\frac{Y_e}{0.5}\right)^{38.1}, \quad (15)$$

$$\dot{Y}_{e,noC} = -0.27\rho_9^{1.90}\left(\frac{Y_e}{0.5}\right)^{39.9}. \quad (16)$$

From the corresponding values of the fitted parameters a, b and C, and equation (14), the final value of the electron mole number of a given mass can be inferred from its location in the plane $\rho_0 - \tau$, that is from its ignition density and hydrodynamical time. The results are shown in Fig. 5. For a supernova explosion model, the actual impact of Coulomb corrections on nucleosynthesis must take into account the expansion of the star previous to the arrival of the deflagration wave. We study this point further in the next section.

4 TYPE IA SUPERNOVAE

The relevancy of Coulomb corrections to the EOS of matter in SNIa models has not been clearly established to date. Owing to the highly dynamical evolution characteristic of the phenomenon, involving large pressure gradients, shock waves, etc., it is not expected that the hydrodynamics of the explosion should be very sensitive to second-order details of the EOS. However, the nucleosynthetic yields can rely much more on the correct treatment of Coulomb corrections. Current models of SNIa give nucleosyntheses that are in gross agreement with what is expected from light curves and spectral observations, and from chemical evolution calculations (Nomoto et al. 1984; Branch et al. 1985; Weaver, Axelrod & Woosley 1980; Hofflich et al. 1997; Kirshner et al. 1993). However, details of the nucleosynthesis, such as relative abundances of the main products of the explosion, are not in fair agreement with Solar system values (Nomoto et al. 1984; Bravo, Isern & Canal 1993; Timmes, Woosley & Weaver 1995). Generally speaking, the nucleosynthesis products obtained in hydrodynamical simulations are too rich in neutronized Fe-peak isotopes, with respect to the main product, ^{56}Fe, which is synthesized in the explosion as the $Z = N$ nucleus ^{56}Ni. Nevertheless, Woosley (1997) turned this weakness of the models into a virtue, by showing that SNIa explosions of C–O white dwarfs at high central densities ($2\text{–}8 \times 10^9\,\mathrm{g\,cm^{-3}}$) are needed to explain the Solar system abundances of some rare Fe-peak nuclei. Woosley (1997) estimated that 2 per cent of the total SNIa explosions should come from white dwarfs in the above density range. From the discussion in the previous section, we can predict two main effects on the nucleosynthesis, caused by the changes in the bulk NSE neutronization rate: first, a larger production of neutronized Fe-peak nuclei, particularly ^{54}Fe and ^{58}Ni, which will make the mean SNIa nucleosynthesis from Chandrasekhar-mass white dwarfs harder to reconcile with Solar system isotopic abundances, and secondly, the rare Fe-peak nuclei accounted for by Woosley (1997) would be synthesized in explosions from lower density, lower mass white dwarfs.

In addition to the effects of Coulomb interactions on SNIa nucleosynthesis through changes in the conductive deflagration velocity and matter pressure, and the effects mentioned in the above paragraph, there is a nucleosynthetic process affected by the inclusion of the electrostatic corrections. This is the α-rich freeze-out of NSE composition, which takes place whenever NSE matter cools below $2\text{–}5 \times 10^9$ K at a density lower than $\sim 10^8\,\mathrm{g\,cm^{-3}}$. In such conditions, the α abundance is high enough for a considerable number of α-capture reactions to take place, changing the final abundance distribution from that in NSE. As the main agent of these reactions is the presence of α, the effect of Coulomb corrections on the α-rich freeze-out can be estimated from their effect on the abundance of α at NSE freeze-out. Fig. 6 shows the abundances in NSE at typical conditions of freeze-out, $\rho = 10^8\,\mathrm{g\,cm^{-3}}$ and $T = 5 \times 10^9$ K, with and without Coulomb corrections. As can be seen, Coulomb corrections lead to a reduction of the abundance of α particles by an amount of order 15 per cent. The main result is that the net amount of α captures also decreases, reducing the final abundance of nuclei such as ^{58}Ni and ^{62}Ni, and allowing more ^{54}Fe to be ejected into the interstellar medium (despite the apparent decrease in ^{54}Fe abundance produced by Coulomb corrections that can be inferred from Fig. 6).

The final effect of Coulomb corrections on SNIa nucleosynthesis must be calibrated with a complete hydrodynamical simulation of the explosion. We computed a deflagration model with (model DF3cc) and without (model DF3id) Coulomb corrections in NSE, and calculated the nucleosynthesis. The physics involved, the method of computation of the hydrodynamical evolution, and the method of calculation of the nucleosynthesis were as in Bravo et al. (1996). The initial model was a C–O white dwarf with a central density of $3 \times 10^9\,\mathrm{g\,cm^{-3}}$. The first mass shell was turned into NSE composition, and the deflagration wave was propagated into the subsequent shells with a velocity taken as the larger of the conductive velocity (given by equation 11) and a turbulent velocity. The details of the algorithm for the calculation of the turbulent flame velocity can be found in Bravo et al. (1996). After a brief period of slow conductive combustion near the centre the flame accelerated, and finally $0.94\,M_\odot$ was incinerated to NSE. The final kinetic energy was 1.05×10^{51} erg, in good agreement

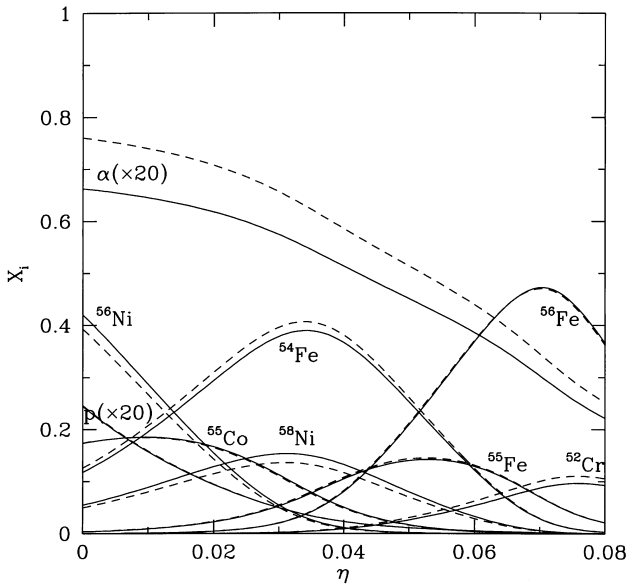

Figure 6. NSE abundances as a function of the neutron excess, with (solid lines) and without (dashed lines) Coulomb corrections to the chemical potentials. The density is $10^8\,\mathrm{g\,cm^{-3}}$.

with what is expected for a typical SNIa explosion. When Coulomb corrections in NSE were dropped (model DF3id), the figures changed to an incinerated mass of $0.93\,\mathrm{M_\odot}$, and a kinetic energy of 1.12×10^{51} erg. The larger kinetic energy for a lower incinerated mass obtained in model DF3id can be understood in terms of the larger pressure exercised by incinerated matter when Coulomb corrections are not taken into account. The mass of radioactive ^{56}Ni freshly synthesized and ejected amounted to $0.57\,\mathrm{M_\odot}$ in model DF3cc, and to $0.58\,\mathrm{M_\odot}$ in DF3id. Thus, no significant differences between the light curves corresponding to the two models are expected.

The location of each mass shell on the expansion time versus ignition density plane is shown in Fig. 5, for model DF3cc only. The position of the mass shells for model DF3id was very similar. As is apparent in the figure, the expansion time was considerable at the beginning of the explosion (central mass shells to the top and to the right), and decreased as more mass was being incinerated. The greatest effect of the inclusion of Coulomb corrections on the neutronization rates can be expected in the central regions, where most neutronized nuclei are synthesized. The actual neutronization reached in the hydrodynamic code was larger than that suggested by the simplified model leading to Fig. 5. Thus, the final electron mole number in the central layer was $Y_\mathrm{e}=0.43\,\mathrm{mol\,g^{-1}}$ in model DF3cc, while it was $0.44\,\mathrm{mol\,g^{-1}}$ in model DF3id. The corresponding figures in the layer $0.1\,\mathrm{M_\odot}$ from the centre were $0.48\,\mathrm{mol\,g^{-1}}$ in both calculations. We now go on to discuss the final nucleosynthesis computed with the full nucleosynthetic code.

The final nucleosynthesis is presented in Fig. 7 for both models, and for the most representative nuclei. Below Ca, either a small mass of each isotope was ejected, or a negligible variation between models was found. The abundances of most isotopes were unaffected by the inclusion of Coulomb corrections. Exceptions were the more neutronized isotopes of each element, for which large increases were found: factors of 10 for ^{48}Ca, 2.6 for ^{50}Ti, 2.3 for ^{54}Cr, 4.7 for ^{64}Ni and 7.8 for ^{66}Zn (although the last two could be affected by the uncertainty of weak interaction

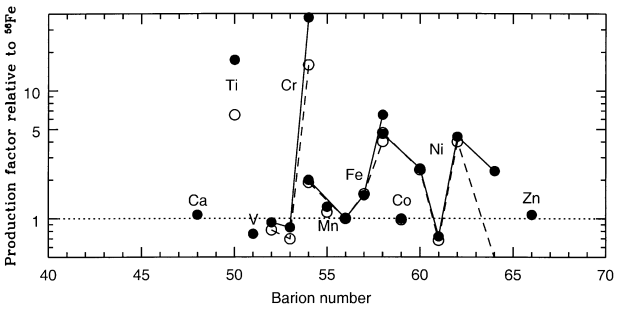

Figure 7. Production factors relative to ^{56}Fe (i.e. abundances relative to ^{56}Fe normalized to Solar system proportions) for models DF3cc (filled circles and solid lines) and DF3id (open circles and dashed lines).

rates above $A=60$). These isotopes were synthesized mainly in a few central layers, where the high non-linearity of the NSE abundance distribution with respect to the neutron excess was apparent. It is interesting to note that the aforementioned increases were obtained with a very modest change in the electron mole number, $\Delta Y_\mathrm{e}=-0.01\,\mathrm{mol\,g^{-1}}$. When compared with models in Woosley (1997), the increases resulting from the inclusion of Coulomb corrections are equivalent to an increase in the central density of the white dwarf at central ignition of order $1-2\times10^9\,\mathrm{g\,cm^{-3}}$. It is also interesting to note that the production factors of ^{54}Fe and ^{58}Ni, as well as those of typical products of α-rich freeze-out, are not sensitive to the inclusion of the corrections. Thus, Coulomb corrections in NSE are not expected to affect the nucleosynthesis from typical SNIa explosions significantly, igniting at $\rho\lesssim2\times10^9\,\mathrm{g\,cm^{-3}}$.

5 ACCRETION-INDUCED COLLAPSE OF WHITE DWARFS

Direct collapse of a white dwarf to a neutron star has been postulated by many authors in order to explain the origin of some low-mass X-ray binary sources (van den Heuvel & Habets 1985; Canal et al. 1990 and references therein), as well as millisecond pulsars (Michel 1987; Baylin & Grindlay 1990). The scenario usually considered consists of a massive white dwarf placed in a compact binary system, accreting matter from a companion at a rate determined by mass ratio and geometric configuration. Low accretion rates ($\dot{M}\lesssim10^{-8}\,\mathrm{M_\odot\,yr^{-1}}$) of H or He, or high accretion rates, near the Eddington limit, of C–O material on to a massive white dwarf can lead to AIC to a neutron star (Nomoto & Hashimoto 1987), especially if the interior of the white dwarf is in a solid state at the beginning of the accretion process (Hernanz et al. 1988). In these cases, explosive central carbon ignition can take place at densities as high as $10^{10}\,\mathrm{g\,cm^{-3}}$. For a fixed initial chemical composition of the white dwarf (C–O, or O–Ne–Mg) there exists a critical density that separates the explosive and collapse outcomes of the ignition. The value of this density is a function of the velocity of the conductive burning front. As a general rule, slow fronts lead to collapse, while fast fronts lead to explosion. The success or failure of the AIC scenario depends on the competition of the pressure rise caused by energy release by the nuclear deflagration front and pressure depletion by electron captures behind the front.

Using the conductive flame velocities uncorrected by Coulomb interactions at finite temperature, Timmes & Woosley (1992) obtained a value of the critical density of $\sim9\times10^9\,\mathrm{g\,cm^{-3}}$ for a C–O white dwarf (Nomoto & Kondo 1991; Canal et al. 1990;

Isern, Canal & Labay 1991). The actual value of the critical density depends on the acceleration of the nuclear flame beyond the conductive velocity by hydrodynamical instabilities, and is affected by the particular modelling assumed for that acceleration. A more fundamental critical density is obtained when one assumes that the flame propagates all the way through the central layers at the conductive flame velocity. Actually, this is what is expected to occur, as the hydrodynamical instabilities need a finite time to develop that is comparable to the time it takes for the white dwarf to decide whether it will collapse or explode (García-Senz, Bravo & Serichol 1998).

The inclusion of Coulomb corrections to the EOS of NSE matter is expected to favour the collapse of the white dwarf, because (1) the conductive flame velocities are lower, (2) the electronic pressures are lower, as a result of the larger bulk neutronization rates in NSE, and (3) the ionic pressures in the nuclear ashes are also lower (the Chandrasekhar mass is reduced). Each of these factors has a separate impact on the value of the critical density, although the net effect of all of them is not the simple sum of each one. We shall now attempt to formulate a crude estimation of the change in the critical density caused by the aforementioned effects. As a zeroth-order approximation one can assume that the critical density is linked to an 'equilibrium' state between the rate at which pressure rises by nuclear burning and the rate at which it falls by electron captures. This 'equilibrium' state is controlled by the burning front velocity, $v_{\rm cond}$, and the NSE neutronization rate, $\dot{Y}_{\rm e}$. Both of them are perturbed by the inclusion of the Coulomb corrections by $\Delta v_{\rm cond} \simeq -0.14 v_{\rm cond}$ and $\Delta \dot{Y}_{\rm e} \simeq 0.28 \dot{Y}_{\rm e}$. Given the dependence of $v_{\rm cond}$ and $\dot{Y}_{\rm e}$ on density, ρ, the 'equilibrium' is re-established for a new density, $\rho + \Delta\rho$, such that

$$\left(\frac{\Delta \dot{Y}_{\rm e}}{\dot{Y}_{\rm e}} - \frac{\Delta v_{\rm cond}}{v_{\rm cond}}\right) + \left(\frac{\partial \ln \dot{Y}_{\rm e}}{\partial \ln \rho} - \frac{\partial \ln v_{\rm cond}}{\partial \ln \rho}\right) \frac{\Delta\rho}{\rho} = 0. \qquad (17)$$

From the discussion in Sections 3.1 and 3.2, and at the high densities we are considering ($\rho \sim 6$–9×10^9 g cm^{-3}), the variation of the conductive velocity and the neutronization rate with density can be well approximated by $v_{\rm cond} \propto \rho^{0.7}$ and $\dot{Y}_{\rm e} \propto \rho^{1.95}$, which leads to $\Delta\rho/\rho \simeq -0.34$. Taking the nominal value of the critical density 8.2×10^9 g cm^{-3}, a new Coulomb-corrected critical density of 5.4×10^9 g cm^{-3} is predicted. Although no more than a crude estimate, the predicted shift of the critical density is in fair agreement with more realistic calculations, as we will show below.

In order to test the consequences of the inclusion of Coulomb corrections for the AIC critical density, we computed a set of models starting at different central densities, and composed of 50 per cent C and 50 per cent O (models CONcc*X* in Table 2, where *X* is to be substituted by the initial central density in 10^9 g cm^{-3}). In all cases, the hydrodynamical calculation started with the incineration of the central layer (2.17×10^{-4} M$_\odot$), and the burning front propagation was followed until the collapse or explosion outcome was clear. The combustion front was assumed to propagate at the conductive velocity. All the models were then recomputed without Coulomb corrections *in NSE* (models CONid*X* in Table 2). In each case, the corresponding conductive velocity was used, either with or without Coulomb corrections at finite temperature, as discussed in Section 3.1. The details of the models, and their outcome, can be seen in Table 2, while the temporal evolution of the central density is shown in Fig. 8.

The effect of the inclusion of Coulomb corrections upon the critical density for AIC, for a purely conductive deflagration, is spectacular. Its value drops from $\sim 8.5 \times 10^9$ g cm^{-3} to $\sim 5.5 \times 10^9$ g cm^{-3}, in agreement with the crude estimation given above. The reduction of the critical density means that in nature there must be more binary systems able to follow the path to AIC than previously thought.

Table 2. Outcome of the hydrodynamic models.

model	$\rho_{\rm c,9}$	corrections	
CONcc5.5	5.5	y	explosion
CONcc6	6	y	collapse
CONcc6.5	6.5	y	”
CONcc7	7	y	”
CONcc8	8	y	”
CONcc9	9	y	”
CONid6	6	n	explosion
CONid7	7	n	”
CONid8	8	n	”
CONid8.5	8.5	n	”
CONid9	9	n	collapse
CONid9.5	9.5	n	”

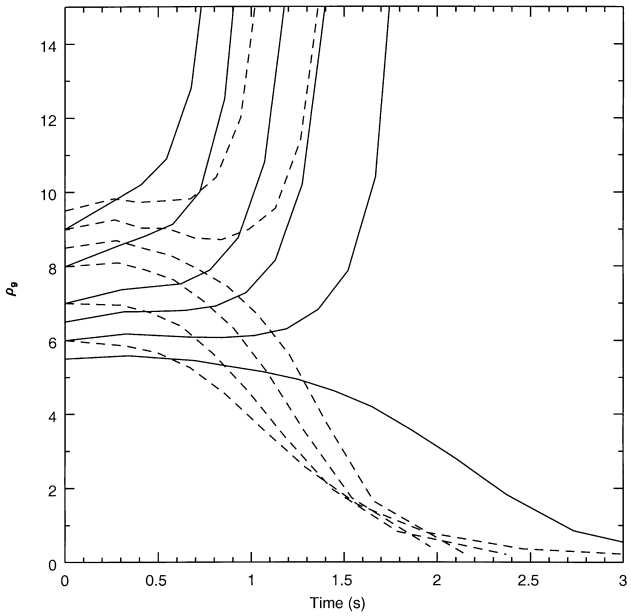

Figure 8. Evolution of the central density of the models in Table 2. Models with Coulomb corrections in NSE are shown with solid lines, while those without the corrections are displayed with dashed lines.

6 CONCLUSIONS

The purpose of the present paper was to examine carefully the effects of the inclusion of Coulomb corrections to the EOS of matter in NSE, at high temperature and density. It has been found that the corrections to the chemical potential have a significant effect on the abundance distribution of nuclei in NSE, favouring high-*Z* nuclei, and equalizing slightly the abundances in the Fe-peak (as Coulomb corrections do not depend on details of nuclear structure, or on nuclear binding energy).

The physics of massive white dwarfs near the Chandrasekhar point was found to be sensitive to the inclusion of Coulomb corrections in NSE in two important aspects. The conductive velocity of a nuclear deflagration front in C–O fell below its nominal value (Timmes & Woosley 1992) owing to the finite-temperature effects on the ionic heat capacity, the reduction being

more important at high densities ($\sim$14 per cent at $\rho \gtrsim 8 \times 10^9\,\mathrm{g\,cm^{-3}}$). The neutronization rate of matter in NSE was modified mainly as a result of the different abundance distribution found after the inclusion of Coulomb corrections. The neutronization rate was increased by about 28 per cent at $\rho = 8 \times 10^9\,\mathrm{g\,cm^{-3}}$ and $Y_\mathrm{e} = 0.5\,\mathrm{mol\,g^{-1}}$. This was a consequence of the greater abundance of nuclei such as Co isotopes, which dominate the neutronization for a wide range of neutron excesses. Modification of the electron capture rate of individual nuclei owing to a shift in the threshold energies was only a second-order effect.

We also performed hydrodynamic simulations of SNIa explosions and of the accretion-induced collapse of a white dwarf, in order to test the relevancy of the above-mentioned effects. A model was computed simulating a deflagration supernova, starting from a central density of $3 \times 10^9\,\mathrm{g\,cm^{-3}}$, and with a flame velocity given by the greater of the conductive velocity and a turbulent velocity. It was found that the hydrodynamic and light curve output was insensitive to the inclusion of Coulomb corrections in NSE. The same applies to the main nucleosynthetic products, such as Si, Fe and most isotopes of Ni. However, some rare nuclei (^{48}Ca, ^{50}Ti, ^{54}Cr, ^{64}Ni, and ^{66}Zn) were largely favoured by the inclusion of Coulomb corrections in NSE, showing increments in their abundances by factors of up to $\sim$10. These nuclei were also identified by Woosley (1997) as products of massive white dwarf explosions, but they can now be synthesized starting from a lower central density white dwarf ($\Delta\rho \sim -2 \times 10^9\,\mathrm{g\,cm^{-3}}$). Of course, our quantitative results depend on the particular explosion model we have computed, but the qualitative behaviour we have outlined is independent of these details.

The impact of the inclusion of Coulomb corrections in NSE on the critical density for AIC of a white dwarf was spectacular. Owing to the combined modification of the conductive velocity (reduced), and the neutronization rate in NSE (increased), a reduction in the critical density of order $\Delta\rho \sim -3 \times 10^9\,\mathrm{g\,cm^{-3}}$ was estimated. A series of hydrodynamical models was calculated starting from different central densities, with and without Coulomb corrections, and followed until it was clear whether the outcome was explosion or collapse. The results agreed with the above estimation of the shift of the critical density. Thus, the value of the critical density for AIC in massive C + O white dwarfs is now set at $5.5 \times 10^9\,\mathrm{g\,cm^{-3}}$.

Our calculations rely on the hypothesis that the Coulomb correction to the free energy for an OCP can be extrapolated with confidence to an MCP, either with the linear approximation or with a 'mean-nucleus' approximation, as in Hansen et al. (1977). We have not attempted to discern whether a different formulation is more appropriate for matter in NSE, characterized by a large number of isotopes with large molar fractions, and in which the nature of nuclei is continuously changing owing to very fast nuclear reactions, but this issue could be a subject for our attention in the future.

ACKNOWLEDGMENTS

This work was supported by the DGICYT grants PB94-0111 and PB94-0827.

REFERENCES

Baylin C. D., Grindlay J. E., 1990, ApJ, 353, 159
Branch D., Dogget J. B., Nomoto K., Thielemann F-K., 1985, ApJ, 294, 619
Bravo E., Isern J., Canal R., 1993, A&A, 270, 288
Bravo E., Tornambé A., Domínguez I., Isern J., 1996, A&A, 306, 811
Bruenn S. W., 1972, ApJS, 24, 283
Canal R., Isern J., Labay J., 1990, ARA&A, 28, 183
Clifford F. E., Tayler R. J., 1965, Mem. R. Astron. Soc., 69, 21
Couch R. G., Loumos G. L., 1974, ApJ, 194, 385
Epstein R. I., Arnett W. D., 1975, ApJ, 201, 202
Fuller G. M., Fowler W. A., Newman M., 1985, ApJ, 293, 1
García-Senz D., Bravo E., Serichol N., 1998, ApJS, 115, 119
Gutiérrez J., García-Berro E., Iben I., Isern J., Canal R., Labay J., 1996, ApJ, 459, 701
Hansen J. P., Torrie G. M., Vieillefosse P., 1977, Phys. Rev. A, 16, 2153
Hernanz M., Isern J., Canal R., Labay J., Mochkovitch R., 1988, ApJ, 324, 331
Hillebrandt W., Nomoto K., Wolff R. G., 1984, A&A, 133, 175
Hix W. R., Thielemann F-K., 1996, ApJ, 460, 869
Hofflich P., Khokhlov A., Wheeler J. C., Nomoto K., Thielemann F-K., 1997, in Ruiz-Lapuente P., Canal R., Thermonuclear Supernovae. Kluwer, Dordrecht, p. 659
Isern J., Canal R., Labay J., 1991, ApJ, 372, L83
Kirshner R. P. et al., 1993, ApJ, 415, 589
Michel F. C., 1987, Nat, 329, 310
Mochkovitch R., Nomoto K., 1986, A&A, 154, 115
Nandkumar R., Pethick C. J., 1984, MNRAS, 209, 511
Nomoto K., Hashimoto M., 1987, Ap&SS, 131, 395
Nomoto K., Hashimoto M., 1988, Phys. Rep., 163, 13
Nomoto K., Kondo Y., 1991, ApJ, 367, L19
Nomoto K., Thielemann F. K., Yokoi K., 1984, ApJ, 286, 644
Ogata S., Ichimaru S., 1987, Phys. Rev. A, 36, 5451
Salpeter E. E., 1957, Comp. Phys., 88, 2
Salpeter E. E., 1961, ApJ, 134, 669
Timmes F. S., Woosley S. E., 1992, ApJ, 396, 649
Timmes F. S., Woosley S. E., Weaver T. A., 1995, ApJS, 98, 617
van den Heuvel E. P. J., Habets G. M. H., 1985, in Srinivasan G., Radhakrishnan V., eds, Supernovae, their Progenitors, and Remnants. Indian Academy of Science, Bangalore, p. 129
Weaver T. A., Axelrod T. S., Woosley S. E., 1980, in Wheeler J. C., ed., Type I Supernovae. University of Texas, Austin, p. 113
Woosley S. E., 1997, ApJ, 476, 801
Woosley S. E., Weaver T. A., 1988, Phys. Rep., 163, 79
Yakoblev D. G., Shalybkov D. A., 1989, Sov. Sci. Rev. E, Astrophys. Space Phys., 7, 311

This paper has been typeset from a TeX file prepared by the author.